

EXPERIMENTAL STUDY INTO THE PERFORMANCE IMPACT OF ENVIRONMENTAL NOISE ON UNDERSEA PULSED LASER SERIAL IMAGERS

Fraser Dalgleish, Anni Vuorenkoski, Gero Nootz, Bing Ouyang, and Frank Caimi

Harbor Branch Oceanographic Institute at Florida Atlantic University
5600 US 1 North
Fort Pierce, FL 34946

(Received April 29, 2013)

This paper examines imaging performance bounds for undersea electro-optic identification (EOID) sensors that use pulsed-laser line scanners to form serial images, typically utilizing one laser pulse for each formed image element. The experimental results presented include the use of two distinct imaging geometries: firstly, where the laser source and single element optical detector are nearly co-aligned (near monostatic); and secondly, to reduce scattering lengths between source and target, albeit with the drawback that the coverage is reduced, the laser source can be deployed on a separate platform positioned closer to the target (bistatic) with the detector being positioned much further from the target. The former system uses synchronous scanning in order to significantly limit the required instantaneous angular acceptance function of the detector and has the desired intention of acquiring only ballistic photons and the undesirable property of acquiring multiple, forward-scattered (snake) photon contributions that indirectly arrive into the detector aperture. The latter system utilizes a staring detector with a much wider angular acceptance function, the objective being to deliver maximum photon density to each target element and to acquire the temporally overlapping diffuse, snake and ballistic photon contributions in order to maximize signal. The study investigates received pulse energy variance from both the direct (target) component and the snake (forward scatter) in clear filtered water, as well as various well-characterized particle suspensions with and without an artificial thin random scattering layer. For each dataset, efforts were made to measure variance due to device shot noise in order to assess the impact of the environment on image quality. The paper provides analytical insight based on test tank experimentation into which configuration of these potentially more compact, more capable EOID systems of the future are more sensitive to two distinct artificially generated scattering conditions (homogenous, high refractive index small particles and a thin layer of inhomogenous large particles with low refractive index), which, in turn, gives a useful indication into how well the various configurations would perform in real conditions.

I. INTRODUCTION

There are a variety of scientific, homeland security, and defense applications for compact *in situ* electro-optic sensors which are effective in identifying and classifying natural and man-made objects in turbid underwater environments. Performance of existing underwater electro-optics sensors is well understood from development of accurate radiative transfer performance prediction models and experimental results obtained in highly controlled testing environments.

Several varieties of underwater electro-optic imaging sensors are currently used, each of which has been engineered to reduce the main mechanisms responsible for loss in image quality due to scattering and attenuation. Laser Line Scan (LLS) underwater imaging is a serial imaging technique which involves the optical scanning of a narrow instantaneous field of view (IFOV) receiver in a synchronous fashion with a highly collimated laser source over a wide swath of

Distribution Statement A: Approved for public release; distribution is unlimited.

Report Documentation Page		Form Approved OMB No. 0704-0188
Public reporting burden for the collection of information is estimated to average 1 hour per response, including the time for reviewing instructions, searching existing data sources, gathering and maintaining the data needed, and completing and reviewing the collection of information. Send comments regarding this burden estimate or any other aspect of this collection of information, including suggestions for reducing this burden, to Washington Headquarters Services, Directorate for Information Operations and Reports, 1215 Jefferson Davis Highway, Suite 1204, Arlington VA 22202-4302. Respondents should be aware that notwithstanding any other provision of law, no person shall be subject to a penalty for failing to comply with a collection of information if it does not display a currently valid OMB control number.		
1. REPORT DATE OCT 2011	2. REPORT TYPE N/A	3. DATES COVERED -
4. TITLE AND SUBTITLE Experimental Study into the Performance Impact of the Environmental Noise on Undersea Pulsed Laser Serial Imagers (U)		5a. CONTRACT NUMBER
		5b. GRANT NUMBER
		5c. PROGRAM ELEMENT NUMBER
6. AUTHOR(S)	5d. PROJECT NUMBER	
	5e. TASK NUMBER	
	5f. WORK UNIT NUMBER	
7. PERFORMING ORGANIZATION NAME(S) AND ADDRESS(ES) Harbor Branch Oceanographic Institute at Florida Atlantic University 5600 US 1 North Fort Pierce, FL 34946		8. PERFORMING ORGANIZATION REPORT NUMBER
9. SPONSORING/MONITORING AGENCY NAME(S) AND ADDRESS(ES)		10. SPONSOR/MONITOR'S ACRONYM(S)
		11. SPONSOR/MONITOR'S REPORT NUMBER(S)
12. DISTRIBUTION/AVAILABILITY STATEMENT Approved for public release, distribution unlimited		
13. SUPPLEMENTARY NOTES See also ADC082395. U.S. Navy Journal of Underwater Acoustics. Volume 61; Issue 4, October 2011- Non-Acoustic ASW, Sensors, Applications.		

14. ABSTRACT

This paper examines imaging performance bounds for undersea electro-optic identification (EOID) sensors that use pulsed-laser line scanners to form serial images, typically utilizing one laser pulse for each formed image element. The experimental results presented include the use of two distinct imaging geometries: firstly, where the laser source and single element optical detector are nearly co-aligned (near monostatic); and secondly, to reduce scattering lengths between source and target, albeit with the drawback that the coverage is reduced, the laser source can be deployed on a separate platform positioned closer to the target (bistatic) with the detector being positioned much further from the target. The former system uses synchronous scanning in order to significantly limit the required instantaneous angular acceptance function of the detector and has the desired intention of acquiring only ballistic photons and the undesirable property of acquiring multiple, forward-scattered (snake) photon contributions that indirectly arrive into the detector aperture. The latter system utilizes a staring detector with a much wider angular acceptance function, the objective being to deliver maximum photon density to each target element and to acquire the temporally overlapping diffuse, snake and ballistic photon contributions in order to maximize signal. The study investigates received pulse energy variance from both the direct (target) component and the snake (forward scatter) in clear filtered water, as well as various well-characterized particle suspensions with and without an artificial thin random scattering layer. For each dataset, efforts were made to measure variance due to device shot noise in order to assess the impact of the environment on image quality. The paper provides analytical insight based on test tank experimentation into which configuration of these potentially more compact, more capable EOID systems of the future are more sensitive to two distinct artificially generated scattering conditions (homogenous, high refractive index small particles and a thin layer of inhomogenous large particles with low refractive index), which, in turn, gives a useful indication into how well the various configurations would perform in real conditions.

15. SUBJECT TERMS

16. SECURITY CLASSIFICATION OF:

a. REPORT

unclassified

b. ABSTRACT

unclassified

c. THIS PAGE

unclassified17. LIMITATION OF
ABSTRACT**SAR**18. NUMBER
OF PAGES**23**19a. NAME OF
RESPONSIBLE PERSON

seabed. It is widely regarded as the optimal technology for extended range underwater optical imaging, with up to 6 attenuation lengths achievable in turbid sea water.^{1,2,3,4} These imagers, which typically utilize moderate-power green continuous wave (CW) lasers, require an adequate laser-receiver separation to reduce the imaging detriment of near-field multiple backscatter. Currently available systems such as AQS-24A are large and require too much power to make them suitable for modern unmanned underwater platforms such as the man-portable autonomous underwater vehicle (AUV). For compact implementations of CW-LLS, the detection of target signals becomes obstructed by temporal overlap from volume scatter in turbid water, as well as loss of dynamic range due to ambient light. To increase their operational range and provide high quality identification-quality imagery, detection methods must be capable of separating the target and volume scattering signals to estimate the energy returning from the target alone. As the system approaches a contrast or power limit, over-sampling techniques, which average many samples for each image pixel, can be used to increase signal to noise ratio and hence improve image contrast, albeit with a reduction of image resolution due to intra-pixel scan and platform motion. Because effective pixel dwell times can be as long as 100 μ s, it is believed that CW LLS systems are more robust to scattering inhomogeneities than the pulsed LLS, which can have effective pixel dwell times of only a few nanoseconds.

Another maturing technique used for extended range underwater imaging systems is range-gating, where the source and receiver are temporally synchronized using a pulsed laser, gated or time discriminating array detector, and knowledge of the time of arrival of the target signal. These methods also have the potential to determine precise distance from the travel time of the light pulses, and from a system packaging perspective, pulsed-gated imager architectures are amenable to a more compact implementation with reduced possible laser-receiver separation. Such techniques can allow separation of the target and scattering volume return signals, thereby increasing the imaging range under certain conditions. Several previous configurations using spatially broadened laser pulses and precisely gated, intensified cameras were built and tested, with results indicating imaging performance beyond 6 beam attenuation lengths.⁴⁻⁹ However, employing wide-angle array detectors, these systems are very susceptible to image degradation due to multiple forward scatter in very turbid water, even when extremely short gate times are used. Furthermore these systems do not offer the wide swath ($\sim 70^\circ$) imagery which LLS systems can provide.

In order to understand the potential for turbid water imaging performance improvement with the pulsed serial imaging alternatives, it is necessary to examine the light propagation process and interactions between photons, the environment, the target and the optical receiver.

Near-Monostatic LLS

The objective of the near monostatic LLS architecture is to maximize photon density on each target element, suppress unwanted backscattered and forward-scattered light, but still collect the image-bearing photons returning from each target element. It accomplishes this by employing a synchronously-scanned collimated laser beam and narrow receiver field of view in a near monostatic configuration. For the results presented in this paper, the separation between the laser source and receiver was 23 cm. Figure 1 shows the general LLS imaging geometry at a single instant during a line scan. It can be seen that many possible paths exist for both direct and scattered light to follow from being emitted from the laser source, to eventually returning to the receiver to form a pixel of the image.

Light which does not make it as far as the target but is still gathered by the receiver is known as backscatter. As shown in Fig. 1, backscatter can be further categorized into light which either takes a multiply scattered 'shortcut' to the receiver or light which is initially scattered in the common volume formed between the laser source and the instantaneous field of view (IFOV) of the receiver. Figure 1 illustrates this phenomena from normalized measured pulse time history plots for both clear water (dark line) and water with high particle concentration (lighter line). The first broad return is due to multiple scattering from particles near the receiver, where the laser energy is greatest. This is followed by the narrower return from common volume backscatter, defined by the intersection of the receiver field-of-view with the laser beam.

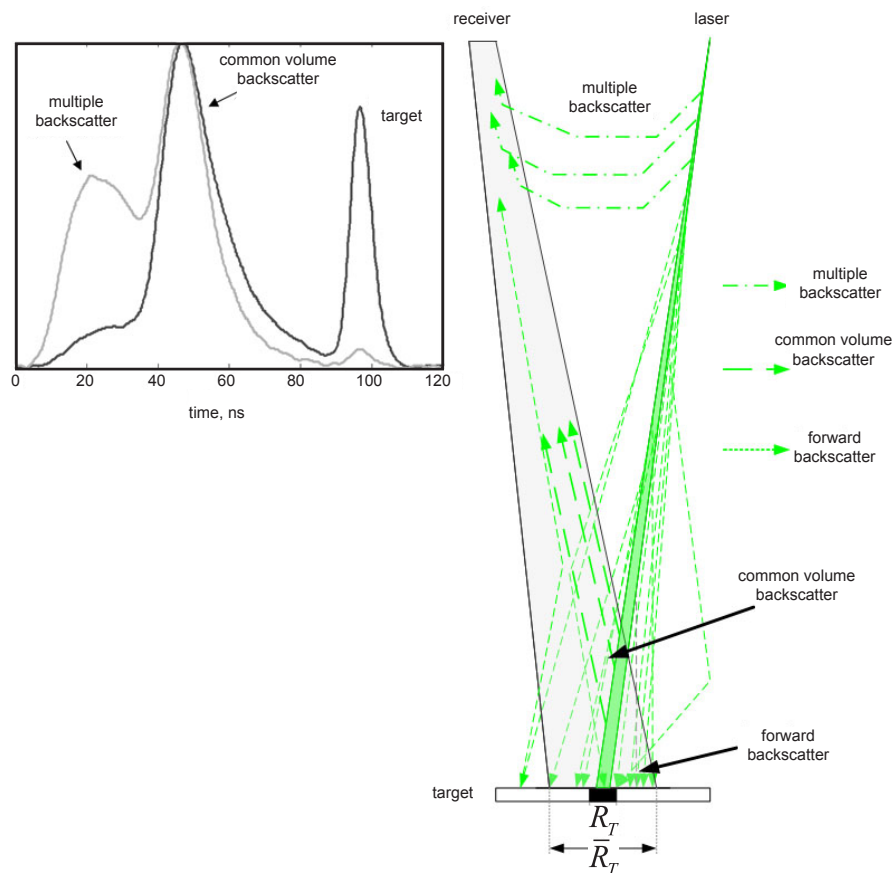


Fig. 1 – Near monostatic LLS imaging geometry at a single instant during a line scan, showing possible routes into the receiver aperture for defined categories of scattered and direct light. Representative normalized laser pulse time-history measurements for two turbidities are also shown. At the higher turbidity (lighter line) the multiple backscatter peak is stronger and the target return is weaker.

Finally, the reflection from the target in the object plane arrives at the receiver. The common volume backscatter peak occurs close to the onset of the common volume region since the intensity of the laser pulse falls off exponentially as it transits the common volume. At higher turbidities, the multiple backscatter return is significant and overlaps the common volume backscatter return.

The effect of backscatter on an acquired image is a reduction in contrast and signal to noise ratio. Backscatter is independent of target reflectance and can be reduced by increasing the source-receiver separation or decreasing the laser and receiver angular apertures. However, as the scattering particle concentration increases, multiple-scattered backscatter levels increase, eventually leading to the contrast limit for a CW LLS system. The time-resolved pulsed LLS allows for removal of the backscatter component using electronic or digital gating.

Not all the light received by an LLS system that has been reflected from the target contains useful information about the region of target being scanned at that instant in time. The component of the received light, which has made it to the target but has undergone scattering with particles on the outgoing path, is known as the forward scattered component. Carrying reflectance information from a larger region of the target R_T (shown in Fig. 1), the main effect of forward scatter on an

acquired image is a reduction in resolution, contrast and signal to noise ratio, particularly when the surrounding target has a high mean reflectance and forward scatter appears as a blurring or glow. For the non-coherent, direct detection pulsed serial imaging systems being discussed in this paper, one possible approach to minimize forward scatter is to reduce laser and receiver angular apertures, but such a scheme has shown to rapidly lead to the system becoming photon deficient in turbid water. Despite the obvious drawback of reducing the scanned swath and hence coverage rate, another possible approach would be to reduce the path length from the laser to the target, *a la* bistatic serial laser imaging, and this is also examined in this paper.

The image component that contains useful reflectance information from the small region of the target R_T (shown in Fig. 1), which is illuminated by the unscattered laser beam, is called the direct component. This consists of light which has not been scattered out of the main beam on the way to the target but can consist of light which has undergone multiple small angle scattering on the way back from the target to the receiver, through those combinations of angles that allow acceptance into the receiver aperture. Allowing for temporal removal of the backscatter component, each pixel formed by the near monostatic pulsed LLS imager consists of the linear superposition of only the direct and forward-scattered components of returning light present at the receiver.

Recent work has focused on investigating time-resolved pulsed LLS techniques, both in simulation¹⁰ and experimentally.¹¹ A pulsed near monostatic LLS radiative transfer model was developed¹² by Metron (Reston, Virginia) that allows the user to configure the medium with depth dependent inherent optical properties (IOPs), and recent studies have been conducted into the effect of thin homogenous scattering layers on image quality, known as the ‘Shower Curtain Effect’;¹³ however, evaluation of the impact of randomly varying scattering layers on image quality is not possible with these models to date.

Bistatic Serial Laser Imaging

Current research also investigates distributed laser serial imaging concepts, which are somewhat unconventional because the imaging system’s components (scanned illuminator and staring receiver) are distributed among multiple platforms. For the purpose of this paper, this type of imaging architecture is known as the ‘bistatic’ geometry. This system configuration was originally demonstrated as a diver-deployed technique in the 1970s.¹⁴ Despite the obvious reduction in swath or coverage by virtue of being closer to the target, this approach has been shown in recent test tank trials to offer a vast range and image quality improvements over single-platform techniques,^{15,16,17} and test tank demonstrated using a communication technique to implement a multistatic configuration which would make it possible to acquire imagery from multiple target sites simultaneously.¹⁸ A Monte Carlo time-resolved radiative transfer model is currently under development by Metron for these more flexibly deployed imaging and non line of sight (NLOS) communications architectures.

In order to better understand the bistatic serial laser imaging technique, it is necessary to examine the light collection process in a turbid water environment. As is the case with all extended range underwater imaging architectures, the objective is to maximize photon density on each target element, suppress unwanted volumetric scatter and forward scatter while still collecting the image-bearing photons returning from the target. The bistatic approach accomplishes this by exercising spatial and angular disparity between source and receiver. For the results presented in this paper, the separation between the source and receiver was almost 11 m. Figure 2 shows the bistatic serial laser imaging geometry at a single instant during a line scan. It can be seen that multiple paths exist for both direct and scattered light as it passes between the laser source to target and from target to receiver. Once again, light which does not reach the target, yet is gathered by the receiver, is considered as volumetric backscatter. In this simplified analysis, any contribution from upwelling or scattered sunlight is not considered, but with wide angle detection receiver configurations, ambient light leakage is a major consideration for daylight operations in shallow coastal waters. This further motivates the use of pulsed laser sources and receiver designs with good out-of-band rejection.

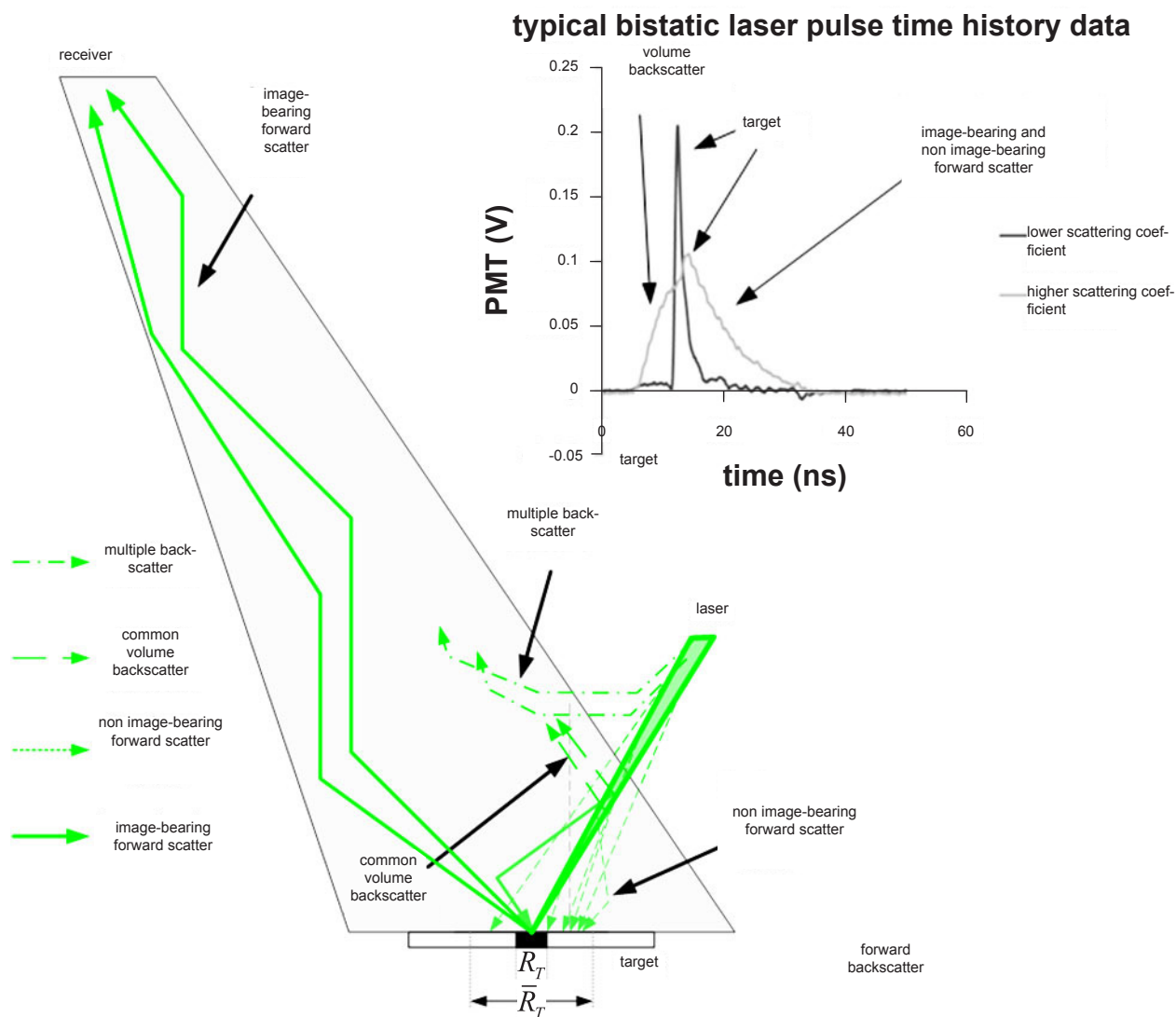


Fig. 2 – Bistatic serial laser imaging geometry at a single instant during a line scan, showing possible routes into the receiver aperture for defined categories of scattered and direct light. A typical bistatic laser pulse time history is also shown for clear water and more turbid water. Source-to-target distance = 2 m; target-to-receiver distance = 10.75 m.

Figure 2 also illustrates this phenomena from measured pulse time history plots for clearer water ($c=0.7 \text{ m}^{-1}$) and also water with high particle concentration ($c=2.5 \text{ m}^{-1}$). In the more turbid case, the first return at the receiver is due to multiple scattering from the common volume and is overlapped by the delayed reflection from target. Multiple scatter also dominates on the return path from the target resulting in the observable 20 ns (4.5 m) tail on the target return. The volume scatter is subject to time delay for the same reason, resulting in volumetric scatter being mixed with the target signal and the forward scatter signal. At higher scattering coefficients, almost all image bearing photons have been scattered multiple times before reaching the receiver.

For the bistatic configuration, temporal separation of the overlapping direct, backscatter and forward scatter signal contributions is not possible, instead the choice of geometry (i.e., positioning the laser transmitter closer to the target) reduces the undesirable signal contributions.

A noticeable attribute of the bistatic imaging geometry in previous turbid water tests¹⁶ was the robustness of image performance in non line of sight (NLOS) geometries, meaning that when there was no direct path between the target and the receiver, image reception was seen to be possible through a wide range of receiver pointing angles; this has potential advantages in deploying a bistatic laser serial imaging system without needing to track transmitter position precisely. For this reason, during the tests described herein, it was also of interest to investigate pulse-to-pulse variance of the target signal in NLOS geometries.

Overview of paper

The experiments described in this paper had the specific objectives of examining the impact of small temporal and spatial scale inhomogeneities in the seawater medium on the imaging performance of one-pulse-per-pixel serial underwater imagers. In natural waters, these inhomogeneities can be attributed to zooplankton, large mineral particles, aggregates, biological scattering layers or turbulence. Previous efforts have focused on investigating performance of CW and pulsed serial imaging techniques in near monostatic geometries, examining degradation due to attenuation, volumetric scatter and forward scatter blur in approximately homogenous scattering suspensions using a high spatial frequency target. Image noise levels for the benchtop pulsed-LLS demonstration¹¹ were significantly influenced by laser energy jitter (>20%), due to limitations with available laser technology, the effect of which was far more significant in clear water. Normalization on a pulse-to-pulse basis using a reference detector is non-trivial and complicates system design. For the experiments described in this paper, a more stable pulsed laser source (< 3% energy jitter) was used, but another objective of the work was to determine what level of laser source pulse energy variance is acceptable for these classes of electro-optic imager. Also of particular interest was to assess the image noise contribution due to the forward scattering component, as it has been found in previous studies¹¹ that the pulsed LLS imager is limited by forward scatter noise. The main effect of forward scattering is a blurring of the image, and this observation agrees with image simulation results. However more knowledge of the variance of that signal component derived from experimental imagery taken in a variety of scattering conditions is desirable. Henceforth, the primary motivation to perform the experiments described herein, was to capture important effects that radiative transfer models cannot currently predict in order to understand limiting factors to allow for better engineering design of future systems.

II. EXPERIMENTAL CONFIGURATION

For both imaging geometries considered, experiments were conducted within the main test tank at the Ocean Visibility and Optics Laboratory at Harbor Branch Oceanographic Institute (Fort Pierce, Florida). These tests consisted of acquiring many single pulse measurements using a large (1.3 m x 1.3 m) static uniform reflectance (estimated reflectance of 70%) test target at realistic stand-off distances (for near monostatic tests, the stand-off distance was 10 meters; for bistatic tests, the laser to target distance was 1.8 meters, and the target to receiver distance was 11 meters) in the alternate geometries (see Fig. 6) through a range of carefully controlled particle suspensions. A 40 μ J 532 nm pulsed laser with 500 ps pulse duration, 500 Hz repetition rate and near diffraction limited beam quality was used for both sets of experiments.

A linear bubble generator was also placed in the tank to provide a simple way to create a random, scattering inhomogeneity into the test volume in a repeatable fashion (see Fig. 3).

An experiment was conducted to measure the average attenuation characteristics of the bubble curtain. The attenuation coefficient was measured with LISST-Stokes (Sequoia Scientific, Bellevue, Washington), a diffraction based laser scattering meter. The transmission measurement of the instrument indicated the attenuation coefficient was between 0.5 and 1.0 m^{-1} at 532 nm.

Ultra-fine Arizona test dust (a high refractive index particle standard with known single scattering albedo and particle size distribution) was used to increase the beam attenuation coefficient (c) values from clear water up to $c=1.02 \text{ m}^{-1}$ at 532 nm (i.e., more than 10 beam attenuation lengths) in several increments for the near monostatic tests. For the

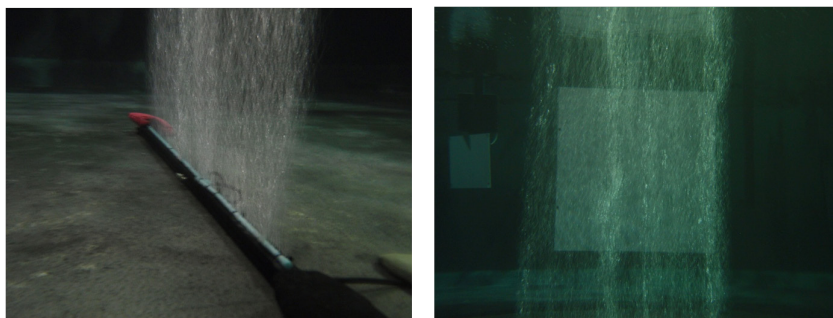


Fig. 3 – Bubble screen in test tank to create a random thin scattering layer

bistatic tests, c values from clear water up to $c=3.13 \text{ m}^{-1}$ were produced (i.e., over 30 beam attenuation lengths). Optical properties were monitored by a Wetlabs ac-9 meter with attenuation and absorption being adjusted for scattering error according to Zaneveld.¹⁹ Single scattering albedo (i.e., the ratio of scattering coefficient to beam attenuation coefficient) was found to be ≈ 0.90 throughout. In addition to measuring beam attenuation and absorption at 532 nm, the forward portion (0° to 7°) of the scattering phase function for the ultra-fine Arizona test dust was measured using the LISST-Stokes. The results are being used in ongoing Monte Carlo simulations of the scenarios.

A microchannel plate (MCP) photomultiplier tube (PMT) (Hamamatsu R5916U-50) was radiometrically calibrated and measured for both impulse response and angular response function for each configuration. A 50 mm diameter plano-convex lens with 100 mm focal length was placed in front of the MCP-PMT. For the near-monostatic configuration a 1.5 mm iris was also placed at the focal point to reduce the FOV. The MCP-PMT was placed a short distance behind the iris to ensure that 60% of the 8 mm active area was being flooded with the defocused light bundle. For the bistatic configuration, the iris was removed. Raytrace modeling results and experimental measurements of the FOV for both configurations were in agreement that the FOV was 15 milliradians ($< 1^\circ$) full angle for the near monostatic experiments and 150 milliradians ($< 10^\circ$) for the bistatic configuration (no iris) both with a flat top angular response.

The range of linearity of the MCP-PMT device was determined experimentally using a variable beam expander and set of calibrated neutral density filters by flooding the photocathode and measuring the peak output current to known input irradiance. This was necessary to establish the linear range of output current from the device during the experiments and also to determine the conversion factor between input peak optical power and measured output peak voltage. The full width at half maximum (FWHM) impulse response of the device was measured at less than 900 ps, which was deemed sufficiently fast to faithfully record the undispersed laser pulse source waveform.

A reference signal was captured using a fast (9 GHz) photodiode detector (EOT-4000) and recorded at 10 GSps. The plot in Fig. 4 represents multiple consecutive pulses overlaid with standard deviation as a percentage of mean for both the integrated pulse energy and the peak value. Neglecting discretization error, this analysis established that the laser source was stable in energy to less than 3%. The noise characteristics of the MCP-PMT at the gain voltage used throughout the experiments were also experimentally characterized as a function of input pulse peak power throughout the linear range of the device. Results from these in air measurements are given in Fig. 5. This is very important for the study described in the paper, since at higher attenuation the device shot noise is expected to be a major contributor to image noise.

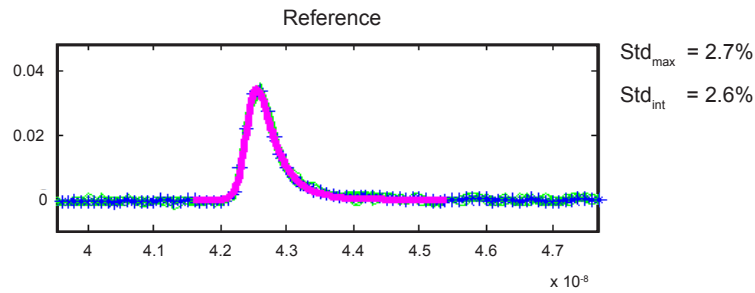


Fig. 4 – Multiple overlaid reference detector signal scope traces (showing < 3% calculated energy variation)

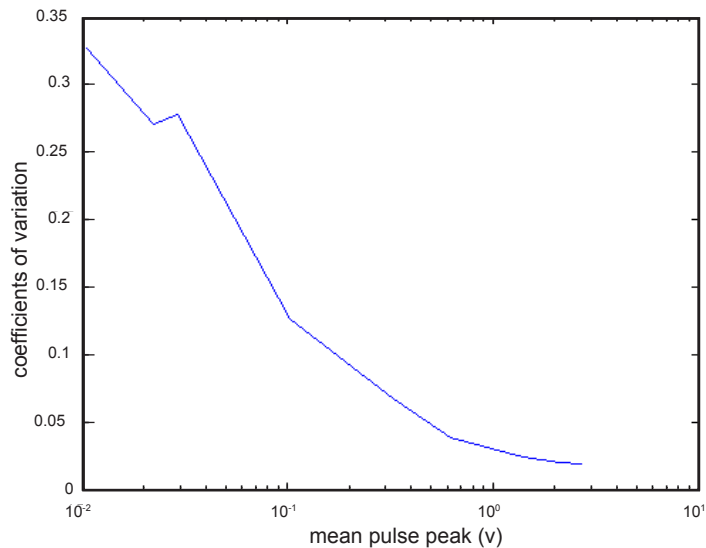


Fig. 5 – MCP-PMT device noise v.s. output voltage

Near Monostatic Experimental Configuration

For the near monostatic tests, the laser and receiver were held stationary throughout. Two sets of experiments were conducted in this configuration. The first experiment attempted to characterize imager noise levels in the time domain by examining statistics of multiple pulse captures during which the medium is the only parameter being varied (turbidity cycle and random scattering inhomogeneity). The second experiment attempts to characterize the imager noise levels by analyzing images formed by precisely moving the target in two dimensions relative to the laser and receiver, much like the image formation process for synchronously scanned laser imager that is being towed through the water.

In the first experiment which had the objectives of characterizing imager noise contributions due to the forward scattering component, also in the presence and absence of a random scattering inhomogeneity, a 1.3 m x 1.3 m target panel was mounted 10 meters from the optical viewport on a linear drive stage for precise positioning (<0.5 mm repeatability). A hole was drilled in the center of the target panel (2.54 cm diameter), which was large enough to pass the laser beam in clear water and also to accommodate the linear drive positional uncertainty. The target was moved perpendicular to the

center of the imager optical axis between two positions, such that in one position the laser beam clearly passed through the hole (determined in clear water), and in another position (20 cm offset) the laser beam was reflected from the solid target panel.

The bubble line (Fig. 3) was placed 2 meters in front of the target. At each turbidity, with and without bubbles, 40 single pulse references, as well as recorded time history returns from the tank, were sampled at 10 Gsps on a 2.5 GHz bandwidth oscilloscope controlled by a LabVIEW program. Figure 6 shows a schematic of the experimental configuration.

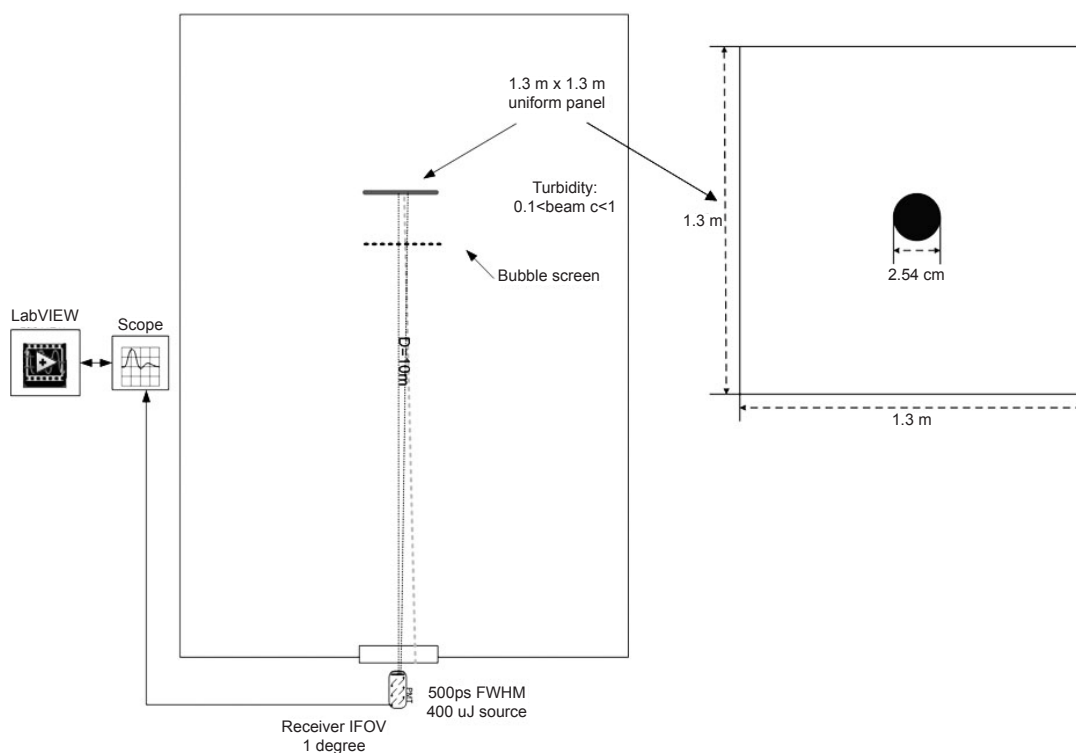


Fig. 6 – Plan view schematic of HBOI large optical imaging test tank configured for near-monostatic tests which had the objective of examining imager noise due to the forward scattering component

In the second experiment, a 20 cm x 30 cm target (Fig. 7) replaced the panel used in the first experiment to conduct an imaging experiment. The target moved at 1 cm interval vertically and horizontally, and at each position, 20 references and return from tank were recorded. At the lowest turbidity ($c=0.085 \text{ m}^{-1}$), data were also taken with the bubble screen in place. Data were recorded at 5 different turbidities ($c=0.085 \text{ m}^{-1}$, 0.389 m^{-1} , 0.625 m^{-1} , 0.825 m^{-1} and 1.02 m^{-1}).

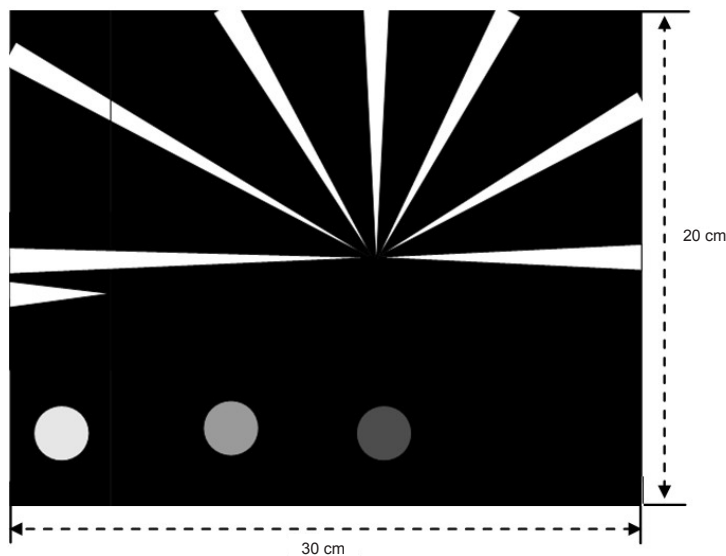


Fig. 7 – Imaging target used in Pulsed Imaging Experiment

Bistatic Experimental Configuration

The bistatic tests had the objectives of characterizing imager noise contributions throughout a turbidity cycle, also as a function of misalignment between the receiver and the target plane and in the presence/absence of a random scattering inhomogeneity. These are practical phenomena that could be experienced during real operations. For these experiments, the laser and same large target panel were held stationary throughout, but the receiver was mounted on a microstepper actuator stage and automatically rotated through a total angle of 68° (-34° to $+34^\circ$) about the line-of-sight (LOS position in 2-degree increments), acquiring 250 single pulse reference and time history datasets at each angular increment, turbidity, and with and without bubbles. The bubble screen (Fig. 3) was also placed 2 meters away from the target in the direction of the receiver. Figure 8 shows a schematic of the experimental configuration.

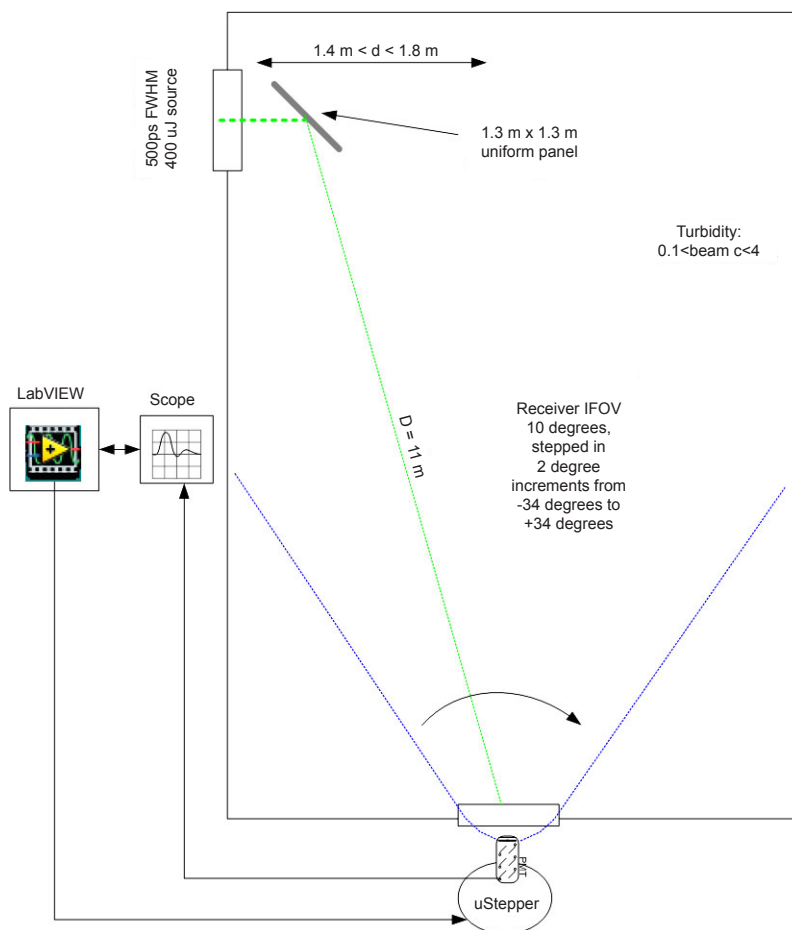


Fig. 8 – Plan view schematic of HBOI large optical imaging test tank configured for bistatic tests

III. RESULTS

In the near monostatic geometry, nine turbidity increments were generated. In an effort to control detector shot noise, which is proportional to the number of received photons, neutral density (ND) filters were used to limit the target signal photon flux and resulting peak current at the receiver for the clearer water cases. The MCP-PMT gain was held constant throughout. Figure 9 shows the mean signal at each turbidity for the non-bubble case. It can be seen that the target signal was held approximately constant by the removal of ND filters from clear water to $c=0.523\text{ m}^{-1}$ (more than five attenuation lengths), beyond which no more filters are present and the target signal became greatly attenuated, eventually reaching a shot noise and power limited scenario at $c=1.02\text{ m}^{-1}$. The data, however does allow evaluation of environmental noise for the cases generated throughout most of the previously observed turbidity operating envelope for this type of sensor (i.e., up to 6 beam attenuation lengths).

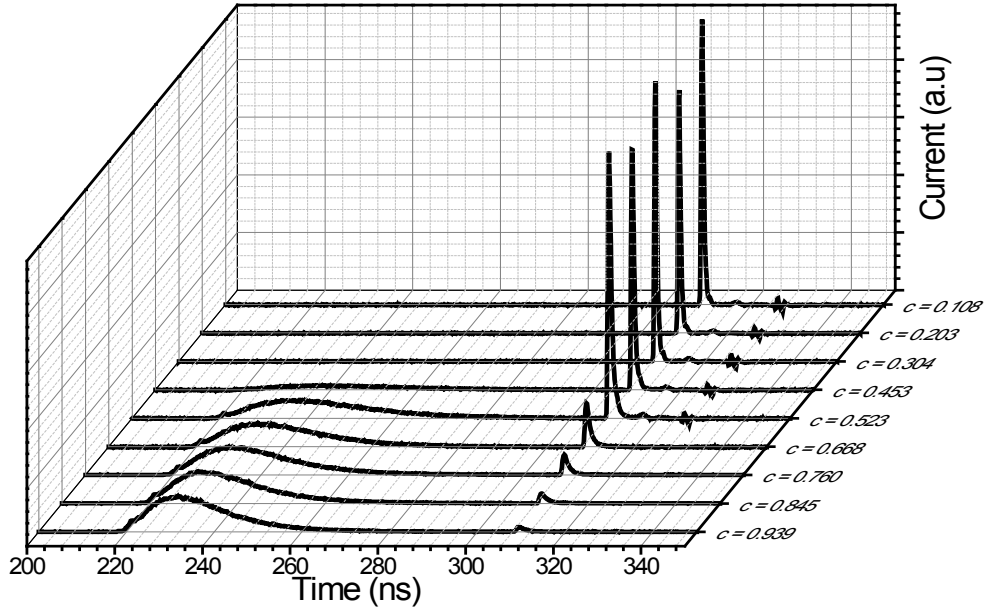


Fig. 9 – Summary of near monostatic experiments showing mean PMT signals for each turbidity without adjusting for ND filter values

Coefficient of Variation (CV), the ratio between the standard deviation σ and mean m : $CV = \sigma / |m|$, were used when studying the noise statistics from the experimental data. Here the mean m is the average of the peaks of the target reflection of the multiple pulses recorded, and σ is the standard deviation of these peaks. For the low turbidity experimental data, the peaks of each of the individual pulses were extracted directly. The location of the peaks were recorded to limit the search range when processing high turbidity data when the volume backscatter dominates the magnitude of the pulses.

The mean pulse peak m and overall pulse-to-pulse standard deviation $\sigma_{overall}$ were computed directly from the data to derive $CV_{overall}$: $CV_{overall} = \sigma_{overall} / |m|$. Under the assumption that the device noise and environment noise are statistically independent, the following formula can be used to compute the standard deviation due to environmental noise using the measured MCP-PMT device noise statistics:

$$\sigma_{environment} = \sqrt{\sigma_{overall}^2 - \sigma_{device}^2} \quad (1)$$

where σ_{device} was computed via interpolation from the MCP-PMT device noise experimental characterization in air (Fig. 5). Subsequently CV due to the environment: $CV_{environment} = \sigma_{environment} / |m|$ was derived.

In the case when the laser was aimed at the solid part of the target panel, for the near monostatic architecture in homogeneous media (i.e., without bubbles), the CV from the target only (for the cases from clear water up to $c=0.523 \text{ m}^{-1}$) was determined as a percentage of the mean to be $\approx 10\%$. This is more than three times the reference pulse energy uncertainty, indicating that the environmental noise dominates the overall imager noise. For the turbidities greater than $c=0.523 \text{ m}^{-1}$, the CV increases as signal photon flux decreases and the device noise started to dominates the overall noise (Fig. 10(a)).

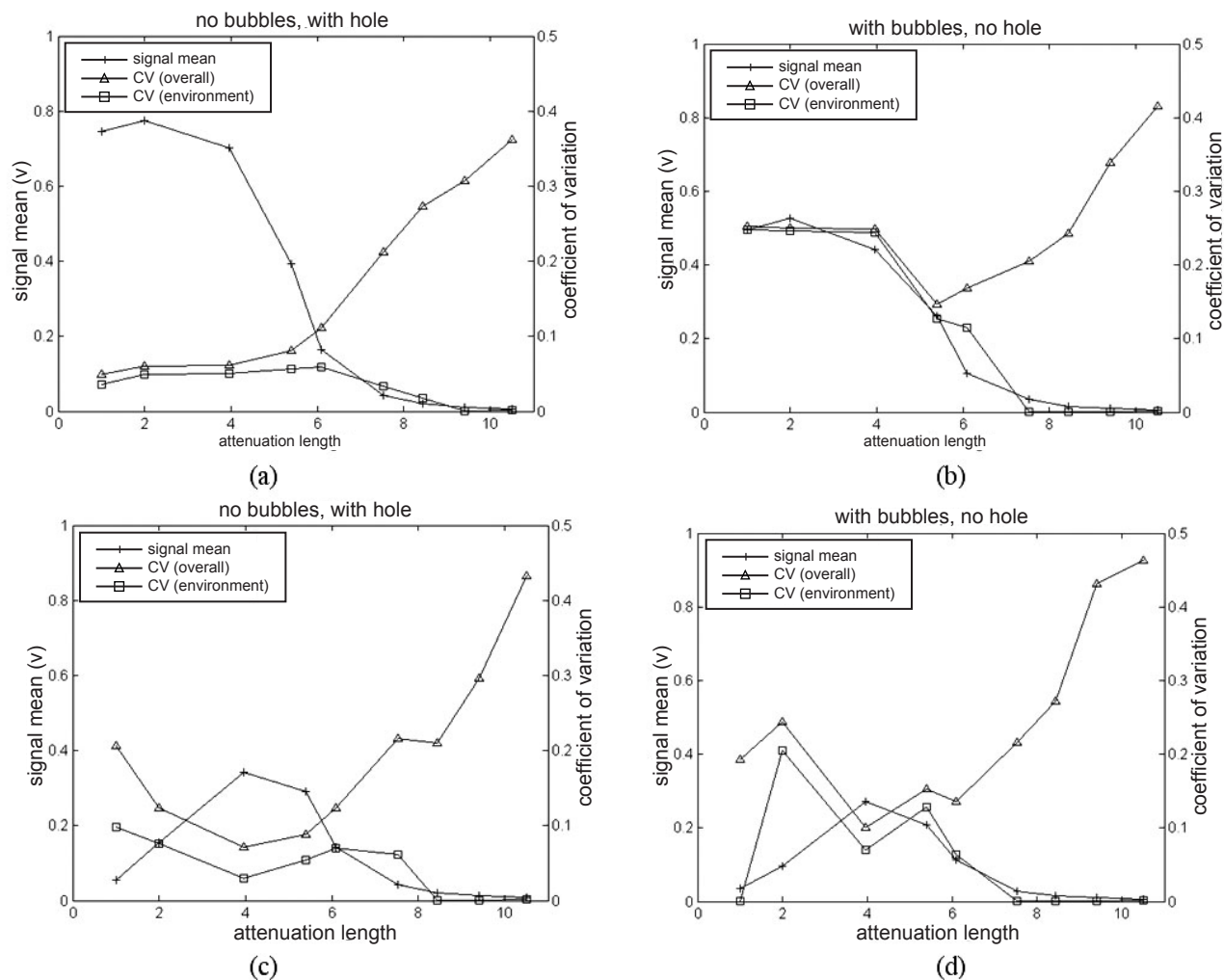


Fig. 10 – Integrated target return energy and standard deviation as a percentage of mean energy for monostatic case with and without bubble curtain as a function of attenuation coefficient

For the inhomogeneous media cases (i.e., with bubbles), the CV of the pulse energy from the target only (for the cases from clear water up to $c=0.523 \text{ m}^{-1}$) was $\approx 25\%$, which is more than six times the reference pulse energy uncertainty. The effect of the bubble curtain randomly scattering, spreading and deflecting the beam has also led to increased attenuation, indicated by the lower signal levels. For the turbidities greater than $c=0.523 \text{ m}^{-1}$, the noise again increases as signal photons decrease (Fig. 10(b)). It can be seen in Figs. 10(a) and 10(b) that the contribution from environmental noise followed the same general trend as in the homogeneous media case.

In the cases that the laser was pointed at the hole, thereby isolating forward scattering from the target signal, shown in Fig. 10(c) and 10(d), it is observed that the strength of the forward scattered target reflection component actually increases with higher turbidity, reaching a maximum at attenuation length = 4, before losing intensity at greater turbidity. The same phenomenon could be observed in both homogeneous and inhomogeneous media cases. This is due to the fact that in this scenario there is no direct (unscattered) reflection from the target because of the hole, and at lower turbidity, the forward scattering signal is weak due to most photons passing through the hole. At increased turbidity, more photons

are spread to nearby elements of the target and were reflected back to the receiver, therefore resulting in increased signal intensity. However, eventually, further increases in attenuation result in less overall photons reaching the target and, therefore, the forward scattering signal diminishes. Regarding the noise distribution, the same trend as in the case of solid panel still held.

These results show that in realistic scattering conditions, even without the artificially introduced large scatterers, the performance up to 5 attenuation lengths is dominated by environmental noise. Beyond this, attenuation and the resulting decrease in signal photons is the reason for device noise being the dominant source of noise, but with a large amount of forward scattering the blur/glow component of the image also becomes the limiting factor for image quality and this has been previously observed with system images.¹¹ It was therefore important to take a set of images to examine the effect of noise in the image domain.

In the near-monostatic pulsed imaging experiment, the images were formed by extracting the target peak from one single pulse at each location to form an image of 30x20 pixels. As mentioned above, the location of the target return at lower turbidity was recorded to be ensure correct peak to be extracted at higher turbidity when the volume scattering dominated. As shown in Fig. 11, the image contrast reduced with increased turbidity as expected, however the image was perceptible until 6.25 beam attenuation lengths.


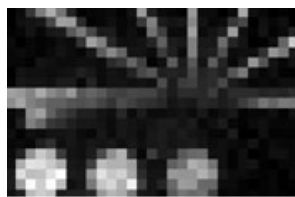
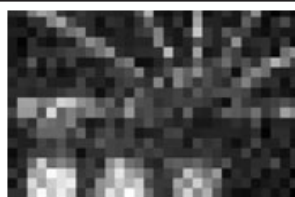
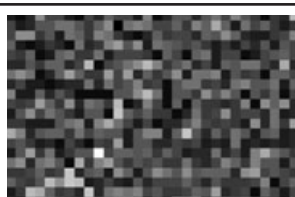
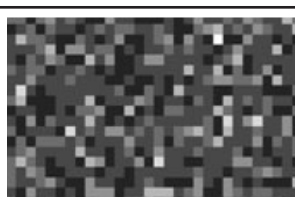
Turbidity	CSNR	Images
0.83	10.1	
3.89	9.301	
6.25	4.24	
8.25	0.5143	
10.2	0.0239	

Fig. 11 – Contrast signal to noise ratio (CSNR) and images from near mono-static pulsed laser line scan imaging (one pixel per pulse) experiment conducted at different turbidities (beam attenuation lengths)

It is also interesting to examine the impact on images when the inhomogeneous scattering layer is generated. As can be seen in Fig. 12, the addition of an inhomogeneous random scattering layer resulted in significant pixel variance, which is most evident when examining the circular 50 mm diameter reflectance standard in the lower left corner. This resulted in much lower contrast signal to noise ratio (CSNR) value. However, it should be noted that the image sharpness is still maintained fairly well, and therefore the overall image quality and hence ability for an operator to identify the object is still greater than for the image taken at 6.25 attenuation lengths despite the CSNR being lower (2.55 versus 4.24). This observation is a good illustration of the distinction of image statistical noise, as being examined in this paper, perhaps not being as significant a detriment for object identification as the blur/glow noise due to forward scattering which is perhaps the primary mechanism for images becoming limited in sharpness and contrast over many attenuation lengths.

For the bistatic tests, which involved the receiver being incrementally misaligned relative to the target (experimental configuration shown in Fig. 8), the peak target signal in the center (LOS) receiver position was again manipulated with ND filters to be approximately constant for five of the eight turbidity steps from clear water up to $c=2.04 \text{ m}^{-1}$. In clearer water, as expected, the signal strength was very weak for the misaligned or non line-of-sight (NLOS) cases. It can also be seen from Fig. 13, that as the turbidity increases, the return signal appears more constant over the angular range of the receiver.

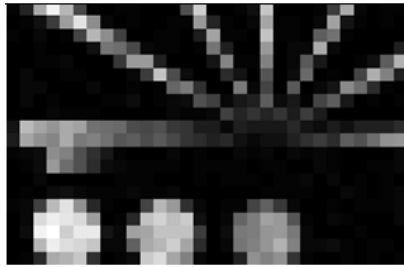
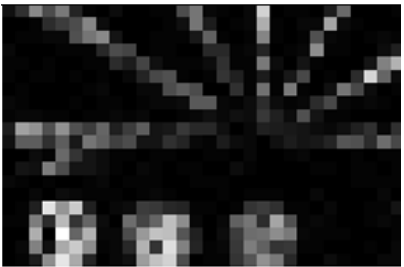
	Without Bubble Screen	With Bubble Screen
CSNR	10.1	2.55
Image		

Fig. 12 – Comparison of CSNR and images of pulsed imaging with and without bubble screen

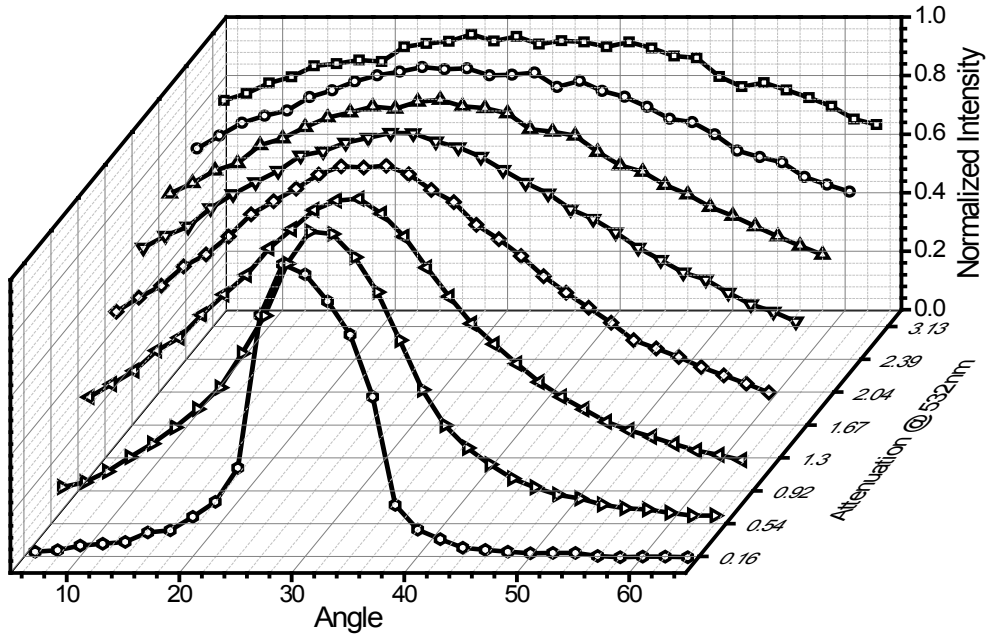


Fig. 13 – Summary of bistatic experiments showing normalized mean PMT signals for each turbidity as a function of angular offset for the non-bubble cases

The analysis of the pulse energy statistics for these bistatic experiments show that, for the clear water cases with the receiver pointing directly at the target (LOS), the derived CV was similar to the laser reference, both with and without the bubble curtain. For the clearer water cases where the receiver was not pointing directly at the target (NLOS), both with and without the bubble curtain, the derived pulse statistics show a greatly increased CV, which is mainly due to the lack of signal and is therefore device noise dominated. However, as the turbidity increased, the CV reduces for the NLOS cases due to multiple scattering leading to more photons arriving at the detector. The effect of the bubble curtain is not very significant for these cases at higher turbidities. Indeed, the CV was observed to remain at 3% for the LOS case through $c=2.39 \text{ m}^{-1}$, gradually spreading out over the NLOS cases with similarly low standard deviation. Figure 14 shows the measured signal mean, CV (overall) and CV (environment) for four different turbidities (beam attenuation lengths = 1.6, 9.2 16.7 and 23.9), with and without bubbles for the entire range of the receiver angular increments. This shows that the distributed laser serial imaging system is more immune to environmental noise and angular misalignment through a wider range of turbidities than the near monostatic case, with the disadvantage that such a configuration will not have the coverage of the near monostatic case.

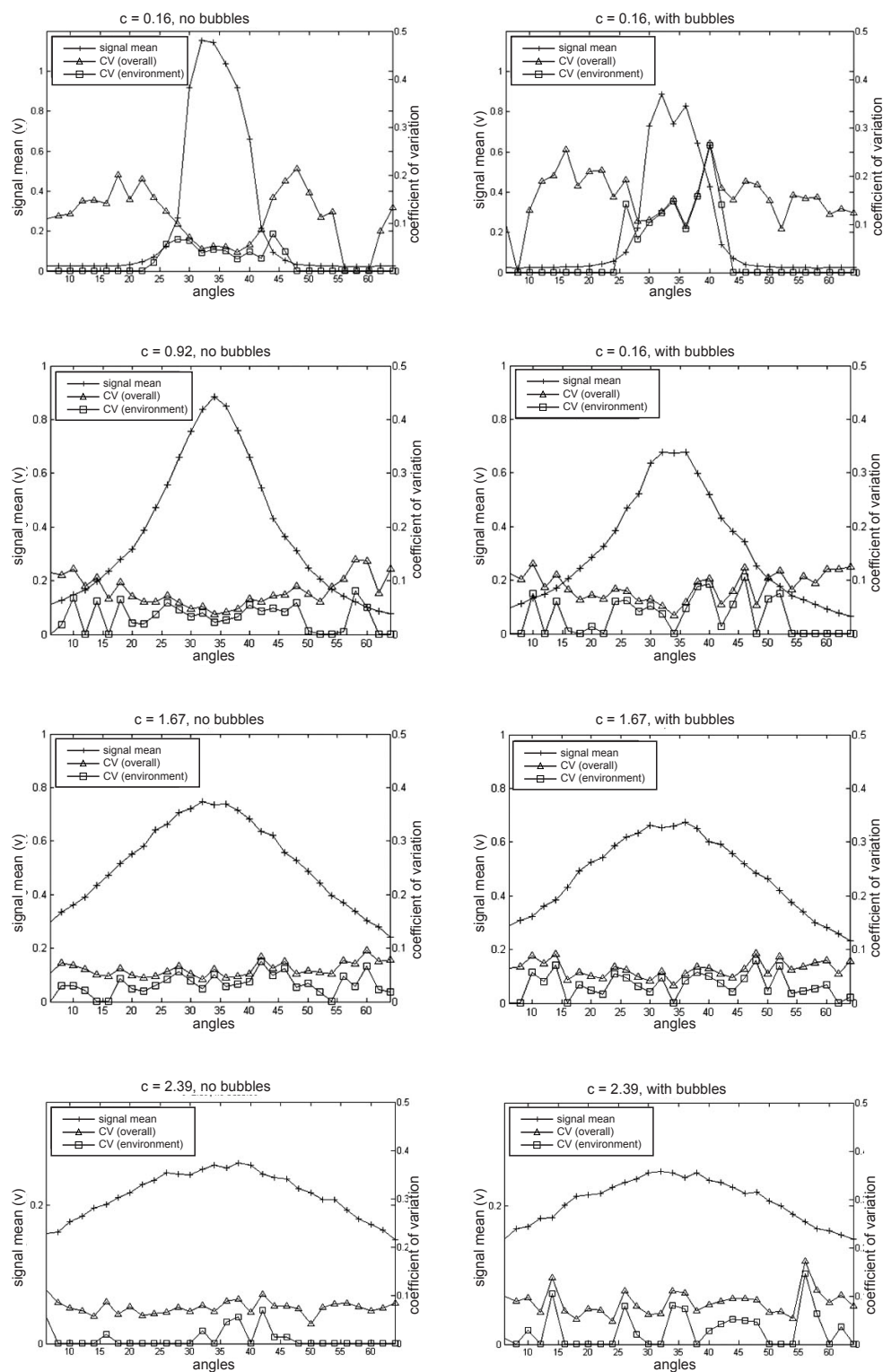


Fig. 14 – Bistatic geometry pulse statistics in clear water case and $c=1.67 \text{ m}^{-1}$ with and without bubbles

IV. DISCUSSION

The results show that in the case of the near monostatic geometry of pulsed laser serial imaging architectures, utilizing narrow angular source and receiver apertures combined with greater signal attenuation on the longer outgoing propagation path, imaging performance is more sensitive to random scattering inhomogeneities than in the case of the bistatic geometry. The pulsed LLS imaging results taken through a range of clear water to more than ten beam attenuation lengths illustrate the distinction between image statistical noise, which is the main emphasis of this paper, and that of forward scattering limiting the contrast and sharpness, and hence ability of an operator to identify small objects (50 mm) from electro-optic imagery. The results show that, in turbid water, pixel-to-pixel intensity noise is not as significant a detriment for object identification as the blur/glow noise due to forward scattering. In clearer water, the effect of large particles or turbulence is perhaps the primary mechanism for images becoming limited in sharpness and hindering identification of small objects.

The distributed configurations of pulsed laser serial imagers, which have demonstrated favorable attributes in turbid water relating to there not being a precise requirement for alignment between the target and the receiver and also, as further elucidated herein, are less sensitive to random scattering inhomogeneities. However, these systems have a major drawback of limited spatial coverage for search and survey applications, something that could be overcome by the use of multistatic system implementation, which has recently been shown to be possible by the authors using frequency division multiple access (FDMA) techniques.¹⁸

To obtain quality imagery from near monostatic imaging systems that exhibit pixel-to-pixel intensity standard deviations of 10% or more will require raw images to be enhanced with computer methods such as deconvolution and other image processing techniques. Alternatively improvements in image quality could be achieved via system designs that use multiple pulses to allow temporal integration or coherent processing, and/or multiple detectors to spatially filter environmental and device noise at the image formation stage.

Multiple receiving systems (diversity receivers) have been used to improve the reliability of wireless communications systems for many years. In such systems, improvement of received signal quality is derived from the existence of multiple signal streams within the communications channel or medium. When signal coherence is maintained through the channel, multiple signals arriving at a single receiver via different paths are subject to fading through coherent combining due to relative time delays through each path. The net effect of using different receivers in the above scenario is to reduce the probability of error essentially by filling in deep fades with signals traveling different paths where destructive interference is less likely, resulting in a net gain, the so-called “diversity gain”. It is therefore of interest to evaluate the potential of such improvement using a receiver consisting of multiple spatially diverged PMTs in an experimental underwater laser imaging/communication system. To that end, the bi-static experimental data were used to compare the CV of averaging of pulses recorded by PMT pointed to three different angles (28, 32 and 36° with that from one PMT at 32°. As shown in Fig. 15, averaging resulted in significant SNR improvement. This observation has inspired the development and deployment of a multiple PMT receiver (Fig. 16).

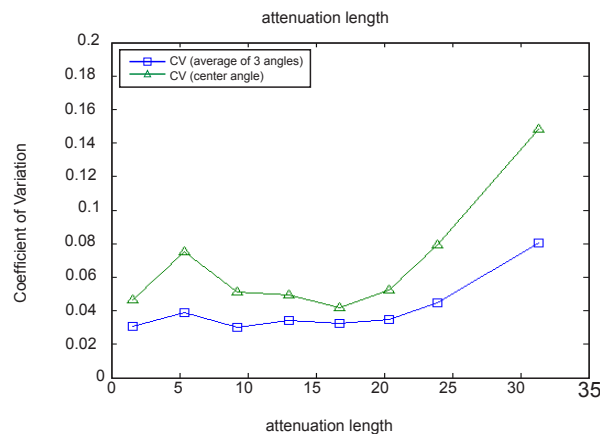


Fig. 15 – SNR improvement via averaging of pulses from multiple PMTs

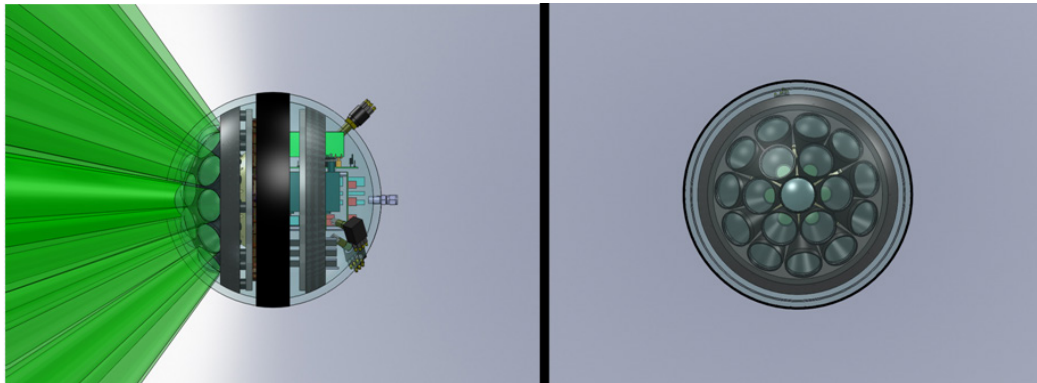


Fig. 16 – Multiple PMT Receiver for Underwater Laser Imaging/Communications

Follow-on to this work would involve better characterization of the bubble curtain IOPs, development of accurate time-resolved radiative transfer code for the bistatic geometry and an accurate detector noise model, which are areas of ongoing research and development for the authors. Apparatus to allow at-sea testing and channel characterization with alternate configurations of pulsed-scanned laser imaging systems in a range natural conditions is currently being prepared.

V. CONCLUSIONS

This work represents a controlled experimental system performance contribution in the growing area of underwater pulsed serial imager system development. The main advantages of using pulsed scanned illumination are in delivering high photon flux to each target element to improve target signal detection in the highly attenuating and scattering environment of natural waters. For daylight systems, pulsed sources offer the possibility to isolate target signals despite DC biases resulting from the presence of ambient light leakage, in order to improve image contrast.

VI. ACKNOWLEDGEMENTS

This work was conducted under a grant monitored by the US Office of Naval Research. This paper is Harbor Branch Oceanographic Institute's contribution number 1834.

VII. REFERENCES

1. M.P. Strand, "Quantitative Evaluation of Environmental Noise in Underwater Electro-optic Imaging Systems," in *Proceedings Ocean Optics XIV*, 1998, Kailua-Kona HI.
2. T.J. Kulp, D. Garvis, R. Kennedy, T. Salmon, and K. Cooper, "Results of the Final Tank Test of the LLNL/NAVSEA Synchronous-Scanning Underwater Laser Imaging System," in *Proceedings Ocean Optics XI*, 1992, pp. 453-464.
3. A. Gordon, "Turbid Test Results of the SM2000 Laser Line Scan System and Low Light Level Underwater Camera Tests," in *Proceedings Underwater Intervention '94: Man and Machine Underwater*, 1994, Washington D.C., (Marine Technology Society) pp. 305-311.
4. M.P. Strand, "Underwater Electro-optical System for Mine Identification," in *Proceedings SPIE 2496*, 1995, pp. 487-497.
5. E.A. McLean, H. R. Burris, and M.P. Strand, "Short-pulse Range-gated Optical Imaging in Turbid Water," *Appl. Opt.* **34**, 4343 (1995).
6. B.A. Swartz, "Diver and ROV Deployable Laser Range Gated Underwater Imaging Systems," in *Proceedings Underwater Intervention '93 Conference*, 1993, New Orleans LA (Marine Technology Society and Association of Diving Contractors).
7. N.H. Witherspoon and J.H. Holloway, "Feasibility Testing of a Range-gated Laser-illuminated Underwater Imaging System," in *Proceedings SPIE Int. Soc. Opt. Eng.* **1302**, 1990, pp. 414.
8. G.R. Fournier, D. Bonnier, J.L. Forand, and P.W. Pace, "Range-gated Underwater Laser Imaging System," *Opt. Eng.* **32**, 2185 (1993).
9. J. Busck, "Underwater 3-D Optical Imaging with a Gated Viewing Laser Radar," *Opt. Eng.* **44**, 116001 (2005).
10. F.M. Caimi and F.R. Dalgleish, 2010, "Performance Considerations for Continuous-wave and Pulsed Laser Line Scan (LLS) Imaging Systems," *J. European Optical Soc.-Rapid Publications* 5, 10020S, (2010).
11. F.R. Dalgleish, F.M. Caimi, W.B. Britton, and C.F. Andren, "Improved LLS Imaging Performance in Scattering-dominant Waters," in *Proceedings SPIE 7317*, 2009, pp. 73170E.
12. T.E. Giddings and J.J. Shirron, "Numerical Simulation of the Electro-optical Imaging Process in Plane-stratified Media," *Opt. Eng.* **48** (12), 126001 (2009).
13. T.E. Giddings and J.J. Shirron, "The Shower Curtain Effect and Electro-optical Imaging Sensors," in *Proceedings Ocean Optics XX*, September 2010, Anchorage AK.
14. B. Ouyang, F.R. Dalgleish, A.K. Vuorenkoski, W.B. Britton, B. Ramos, and B. Metzger, "Visualization for Multi-static Underwater LLS System Using Image Based Rendering," Submitted to *IEEE Oceanic Engineering*, 2011.
15. L.J. Mullen, A. Laux, B. Conconour, and W. McBride, "Extended Range Underwater Imaging Using a Time Varying Intensity (TVI) Approach," in *Proceedings Marine Technol. Soc./IEEE Oceans Conference*, 2009, Biloxi, MS (IEEE, New York, NY).

16. S.Q. Duntley, R.W. Austin, R.L. Ensminger, T.J. Petzold, and R.C. Smith, "Experimental TVI System Report," Visib. Lab. Tech. Rep., pp. 74-1, 1974.
17. F.R. Dalgleish, F.M. Caimi, A.K. Vuorenkoski, W.B. Britton, and B. Ramos, "Experiments in Bistatic Laser Line Scan (LLS) Underwater Imaging," in *Proceedings Marine Technol. Soc. IEEE Oceans Conference*, 2009, Biloxi MS (IEEE, New York, NY).
18. F.R. Dalgleish, B. Ramos, W.B. Britton, and F.M. Caimi, "Multistatic Distributed Laser Line Scan Underwater Imaging Architecture," in *Proceedings Ocean Optics XX*, September 2010, Anchorage, AK.
19. J.R.V. Zaneveld, J.C. Kitchen, and C. Moore, "The Scattering Error Correction of Reflecting-tube Absorption Meters." in *Proceedings Ocean Optics XII SPIE*, 1994, 2258: 44-55.

Dr. Fraser Dagleish directs the Ocean Visibility and Optics Laboratory at Harbor Branch Oceanographic Institute. He is currently chair of the Underwater Imaging Committee at Marine Technology Society. His research emphasis is on undersea laser sensor development, both for remote and in situ environmental measurements and to improve sensing and communications capabilities as an enabling technology for multi-vehicle imaging and sensing operations. Recent development activities in collaboration with government and industry have focused on new laser instrumentation, simulation tools and detection approaches for ocean sensing and monitoring applications. Projects within academia involve collaboration with scientists in sensor package development and ocean observatories for water quality monitoring and imaging missions. Dr. Dagleish earned his Ph.D. degree in Ocean Engineering from Cranfield University in 2004.

Dr. Anni Vuorenkoski is with the Ocean Visibility and Optics Lab at Harbor Branch Oceanographic Institute at Florida Atlantic University. Her current research concentrates on the characterization of water column and benthic features by polarimetry, fluorometry, angularly-resolved scattering techniques, and LIDAR methods, as well as on the experimental validation of computational radiative transfer models. Dr. Vuorenkoski earned her Ph.D. degree in Mechanical Engineering from Cranfield University in 2004.

Dr. Gero Nootz received his Ph.D. in Physics from the University of Central Florida. He joined the Ocean Visibility and Optics Lab at Harbor Branch Oceanographic Institute at Florida Atlantic University in 2010 as a postdoctoral investigator. His current research interest is centered on measuring, understanding, and modeling of the influence optically active turbulence has on image formation and optical line of sight communication in the ocean.

Dr. Bing Ouyang joined the Ocean Visibility and Optics Lab at Harbor Branch Oceanographic Institute at FAU in 2009. His current research interests include underwater computer vision, novel underwater electro-optical system design, underwater LIDAR imaging enhancement, pattern recognition and analysis for sensor time series data. Prior to joining HBOI, Dr. Ouyang was with Texas Instruments, Inc. (TI) from 2003-2009; and he was an algorithm engineer with the DLP ASIC algorithm team, with the primary focus in developing front end algorithms for the video processing ASIC. He received his Ph.D. degree in Electrical Engineering from Southern Methodist University in 2007 while working at TI. Dr. Ouyang is a recipient of the 2013 Young Investigator Research Program award. He holds five U.S. patents in the area of analog video and graphics format detection. He was peer elected to the TI's Member of Technical Staff. Dr. Ouyang is a member of IEEE.

Dr. Frank Caimi has served as a consultant to government and industry for over 30 years in the areas of imaging, image processing, signal processing, pattern recognition, communications, and display technology, and holds patents relating to image formation systems, lighting control, optical sensors, electromagnetics, and measurement devices. Dr. Caimi is editor Society of Photo-Optical Instrumentation Engineers (SPIE) Milestone Series "Underwater Optics" and has authored several book chapters in related subjects. He has led numerous research and development programs for various government sponsors, including NSF, ONR and DARPA and is a senior member of the IEEE, and serves as a Technical Chair in Underwater Optics for the IEEE Oceanic Engineering Society.